Nuclear Materials and Energy 34 (2023) 101365

Contents lists available at ScienceDirect

Nuclear Materials and Energy

journal homepage: www.elsevier.com/locate/nme

Investigation of the dependence of $p_{e,ped}$ on $n_{e,sep}$ in JET H-Mode plasmas using integrated JETTO-MISHKA-FRANTIC simulations

J. Simpson [a,b,*], D. Moulton [a], C. Giroud [a], M. Groth [b], L. Horvath [a], F.J. Casson [a], F. Kochl [a], L. Frassinetti [c], G. Corrigan [a], S. Saarelma [a], L. Garzotti [a], D.S. Gahle [d], A. Chankin [e], JET contributors [1]

[a] CCFE, Culham Science Centre, Abingdon, OX14 3DB, UK
[b] Aalto University, FI-00076 AALTO, Espoo, Finland
[c] Division of Fusion Plasma Physics, Royal institute of Technology (KTH), Stockholm SE, Sweden
[d] University of Strathclyde, 16 Richmond St, Glasgow G1 1XQ, UK
[e] Max–Planck-Institut für Plasmaphysik, Boltzmannstraße 2, D-85748 Garching, Germany

ARTICLE INFO

Keywords:
Pedestal stability
Pressure pedestal
Core edge integration
EPED
JINTRAC

ABSTRACT

Experimentally, it has been observed in high-confinement (H-Mode) plasmas with Edge Localised Modes (ELMs) on JET that the pressure pedestal ($p_{e,ped}$) is degraded by approximately a factor of two when there is a change in electron separatrix density, $n_{e,sep}$, from $1-4\times10^{19}\ m^{-3}$. Previous work using the pedestal stability code EUROPED, has been able to predict the degradation of $p_{e,ped}$ but only for $n_{e,sep} \leq 1.5\times10^{19} m^{-3}$. In this work, we apply a coupled code JETTO-MISHKA-FRANTIC, to self-consistently predict the transport in the pedestal region and neutral source with varying separatrix conditions. The code feeds back on the transport in the pedestal region to achieve profiles that are marginally stable to ideal MHD modes (continuous ELM model in JETTO).

When accounting for the change in electron separatrix temperature ($T_{e,sep}$), ion separatrix temperature ($T_{i,sep}$) and the poloidally integrated neutral flux crossing the separatrix ($\Gamma_{sep,neut}$) as it changes with $n_{e,sep}$ (according to a scan in $n_{e,sep}$ in the edge code EDGE2D-EIRENE), no degradation in $p_{e,ped}$ was observed in JETTO-MISHKA-FRANTIC in contrast to experiment. Instead, an increase in $p_{e,ped}$ with $n_{e,sep}$ was observed which is driven by an increasing density pedestal ($n_{e,ped}$). Within the presented JETTO-MISHKA-FRANTIC simulations, changing the pedestal width by a factor of two and a half in normalised poloidal flux (ψ_n) resulted in an approximately 40% degradation in $p_{e,ped}$ for $n_{e,sep} = 1-3\times10^{19}\ m^{-3}$. This change in pedestal width was not supported by experimental data. A scan in the ratio of particle and energy transport in the pedestal (D/χ) was found to have a negligible effect on $p_{e,ped}$. Qualitative agreement between JETTO-MISHKA-FRANTIC with EUROPED was found when the input density profiles are identical.

1. Introduction

Within the confined plasma region, there is a steep gradient region, known as the pedestal. This pedestal exists in the temperature and density (and thus pressure) profiles and is quantified by the pedestal height and pedestal width. Typically, increases in the height of the pressure pedestal ($p_{e,ped}$) lead to an increase in the core pressure due to 'stiff' profiles [1] which means the normalised temperature and density gradient remain constant in the core — leading to an increase in the fusion power [2]. Therefore, future reactors will want to aim for the largest $p_{e,ped}$ possible to increase fusion performance. Furthermore, future reactors will also require divertor detachment in order to achieve tolerable heat fluxes to the targets [3]. Typically, higher midplane separatrix densities ($n_{e,sep}$) leads to a more detached divertor and hence a reduction in heat flux to the targets [4,5].

Experimentally, in plasmas with low triangularity (δ) plasmas $n_{e,sep}$ is negatively correlated with the electron pressure pedestal $p_{e,ped}$. This behaviour has been observed in JET (for plasma currents $I_p \leq 2.5\ MA$) [6,7], ASDEX Upgrade [8] and D-IIID [9]. $n_{e,sep}$ is correlated with divertor detachment [4] and $p_{e,ped}$ with fusion performance. These experimental results show a trade-off between a feasible divertor solution, where detachment is the priority, and a pedestal solution which is optimised for fusion performance.

* Corresponding author at: CCFE, Culham Science Centre, Abingdon, OX14 3DB, UK.
E-mail address: james.simpson@ukaea.uk (J. Simpson).

[1] See the author list of 'Overview of JET results for optimising ITER operation' by J. Mailloux et al 2022 Nucl. Fusion 62 042026.

https://doi.org/10.1016/j.nme.2023.101365
Received 30 June 2022; Received in revised form 6 January 2023; Accepted 9 January 2023
Available online 20 January 2023

Peeling-Ballooning (PB) modes [10] are believed to be the ultimate instabilities that limit the height and width of the pedestal and thus $p_{e,ped}$. In JET-ILW (ITER like wall) discharges at low $n_{e,sep}$ ($\lesssim 1.5–2 \times 10^{19}$ m^{-3}) PB modes have been found to be marginally stable just before an edge localised mode (ELM) crash in JET [6,7,11]. Moreover they have also been shown to limit the pedestal growth in ASDEX Upgrade [12] and DIII-D [13]. PB modes are an ideal MHD instability and can be predicted by MHD stability codes such as ELITE [14] and MISHKA [15]. Routinely, codes like EUROPED [16] that integrate ideal MHD stability codes with models for the pedestal widths, e.g. the EPED scaling [17] have been used to predict pedestal widths and heights.

The EUROPED model [16] has been able to reproduce the experimentally observed degradation of $p_{e,ped}$ with $n_{e,sep}$ but only at low $n_{e,sep} \leq 1.5 \times 10^{19}$ m^{-3} in JET [6]. In this work EUROPED used the EPED scaling [17] to calculate the width of the pedestal. The work of T. Luda et al. [18] used a pedestal width model that scales as $\nabla(T_e)/T_e$ (where T_e is the electron temperature in the pedestal) and a model to predict $n_{e,sep}$ based on a neutral flux input from the user. This model was able to accurately reproduce the $p_{e,ped}$ degradation with $n_{e,sep}$ on ASDEX Upgrade. These results determined that as $n_{e,sep}$ increases, the position of the maximum pressure gradient moves towards the separatrix, which causes the destabilisation of the PB modes.

In this paper, we present an $n_{e,sep}$ scan using the simulation code JETTO-MISHKA-FRANTIC in an attempt to simulate $p_{e,ped}$ degradation with $n_{e,sep}$ (which has been experimentally observed on JET). The code consists of a coupled core (Bohm Gyro-Bohm) and pedestal transport model (JETTO), in which the pedestal transport is governed by an ideal MHD stability code (MISHKA) and a neutral model (FRANTIC), which has been used to self-consistently predict the density. Within JETTO-MISHKA-FRANTIC we self-consistently evolve the neutral source with the separatrix boundary conditions, which is a step beyond previous works [6] which assumed a fixed density profile and non-varying separatrix conditions.

2. Simulation set up

2.1. Code coupling

The coupled JETTO (core 1D transport code), FRANTIC (neutral code), HELENA (fixed boundary axi-symmetric Grad-Shafranov equilibrium code) and MISHKA (ideal MHD stability code) have been used to perform a scan in $n_{e,sep}$ to predict $p_{e,ped}$. A break down of each code and how it is coupled is given below:

1. *PENCIL* [19]. This module calculates the neutral beam deposition source of both particles, current and power, based on the Neutral beam (NBI) heating scheme employed.
2. *FRANTIC* [20]. An atomic neutral code that calculates the ionisation source based on a user-specified atomic neutral source, or it can be configured so that a particular $n_{e,ped}$ is achieved by automatically adjusting the neutral source. In both cases, the neutral atomic temperature was set to 300 eV; we find a weak sensitivity of the predicted density profile to the neutral temperature [21].
3. *JETTO* [22]. JETTO predicts the temperature, density, and current profiles using the selected transport model and applying the beam source provided by PENCIL, the ionisation source predicted by FRANTIC, the separatrix boundary conditions $T_{e,sep}$, $T_{i,sep}$, $n_{e,sep}$ and the total current. In this setup, Bohm Gyro-Bohm (BgB) transport was used for the core transport model [23]. The pedestal transport model is described in Section 2.3. The current is diffusive and the contribution of the bootstrap current is calculated by a neoclassical solver — NCLASS [24]. The simulation resolution was 300 grid points that are equally spaced in poloidal flux, which is approximately a grid point every 2.7 mm.
4. *HELENA* [25]. HELENA is an axi-symmetric Grad-Shafranov equilibrium solver which takes the pressure and current profiles from JETTO and generates a high resolution equilibrium to be used in ideal MHD stability analysis. Only if stated, HELENA can also take the temperature and density as inputs from JETTO and calculate the total current profile itself (rather than taking it from JETTO) utilising the Sauter formula [26,27] to calculate the bootstrap current contribution.
5. *MISHKA* [15]. MISHKA is an ideal MHD stability code, which takes the equilibrium calculated by HELENA and calculates its ideal MHD stability. MISHKA is only run in the pedestal region, and in this setup calculates whether the equilibrium is unstable to the following toroidal mode numbers (n) - $1, 3, 5, 7, 9, 12, 15, 18, 21, 25$. MISHKA is run at a resolution of 252 points and the number of poloidal harmonics (m) used for each n number is as follows: $m = 30$ for $n = 1$–10, $m = 70$ for $n = 10$–30, $m = 90$ for $n > 30$ which is similar to that used in EUROPED [16]. Checking larger m value for increasing n is imperative for capturing whether high n (> 15) modes are unstable. For each n a growth rate (γ) is calculated. The equilibrium is deemed unstable to a specific n if $\gamma^2 \geq 0.03\ \omega_A$ where ω_A is the Alfven frequency. The mode (n) which satisfies both $\gamma^2 \geq 0.03\ \omega_A$ and has the largest γ of all the modes checked is deemed the most unstable mode.

2.2. JET discharge details

The pedestal profiles in density and temperature are measured using the Thomson scattering system on JET [28]. To calculate the height and width of the pedestal, the modified tanh (mtanh) function was applied to the Thomson scattering data [28,29]. Modified tanh pedestal fits for the JET discharge 96 202 with $I_p = 2\ MA$, $B_t = 2.3\ T$ ($t = 50.56$ s) were taken as the initial condition of the simulations. This discharge was selected because previous work of Ref. [6] used this discharge in EUROPED simulations which we directly compare to in this work. Furthermore, the profiles for this discharge were close to the ideal MHD PB stability boundary. Hypothetically, this means that the time evolution of the profiles in JETTO would quickly evolve to the PB limit. Hence, the computational time to convergence should be short compared to starting with profiles which are further away from the ideal MHD stability boundary. It should be noted that the equilibrium used in JETTO does not evolve and is taken from EFIT [30] at $t = 50.56$ s. However, the equilibrium that is passed to MISHKA from HELENA evolves with the temperature, density, and current profiles predicted by JETTO.

2.3. Description of the continuous ELM model

In the presented JETTO simulations the domain consists of two regions; the core and the edge transport barrier (ETB). The ETB width within the simulation can evolve via the EPED scaling [17], or it can remain fixed. Transport in the core region is assumed to be Bohm - Gyro-Bohm (BgB), which is typically used for JET H-mode plasmas [31]. The diffusive transport coefficients in the ETB region in the particle channel (D) and the heat (ion & electron) channel (χ) are evolved in time, hence changing the pedestal height (and sometimes the pedestal width). The ideal MHD stability of these predicted profiles is then calculated by MISHKA. Once the profile is found to be ideal MHD unstable, the values of D and χ in the ETB region increase so that the height of the pedestal is reduced. The width of the ETB region will either be predicted by the EPED scaling or remain at a fixed width as set by the user. D and χ are increased until the pressure profile becomes ideal MHD stable. At all times, the value of D/χ is kept constant to a user-defined value, which in these simulations is $D/\chi = 1/20$ (informed by Ref. [32]) unless otherwise stated. This process of changing the transport occurs regularly over the time evolution of the simulation. The aim is to achieve a steady state such that the JETTO values of the

electron temperature, density, and pressure at the pedestal converge to an approximately constant value as a function of time. By "pedestal values" here, we mean the values at the innermost edge of the ETB imposed in the simulations. This is akin to the pedestal profiles being held very close to the PB stability boundary. This is then deemed to be the converged profile/pedestal values and is what is presented in the following sections. This is the "continuous ELM model" in JETTO and further details of its mechanics are given in Refs. [33–35]. Note that in all the presented simulations the temperature and density ETB widths are assumed equal. The method of how the D and χ profiles are varied in the ETB region is given by Equation (2) in Ref. [33]. In this equation, the user sets the parameters C_{1-3} in JETTO ($C_1 = C_2$ in this work) and the ratio of these parameters is normally stated as $D/\chi = C_3/C_1$.

2.4. The simulation setups

Three different simulation setups are used in Section 3. For all setups, beryllium is included as impurity and the effective Z (Z_{eff}) is set to $Z_{eff} = 1.2$ and no relationship between $n_{e,ped}$ and $n_{e,sep}$ is assumed.

- **S.1** This simulation setup was used to compare JETTO-MISHKA and EUROPED. The density profile is fixed; only the temperature and current profiles are solved for. The ETB width was evolved according to the EPED scaling [17] and $T_{e,sep} = T_{i,sep} = 100$ eV. Only the temperature (and hence $T_{e,ped}$) is predicted by JETTO and further (only in this particular simulation setup) HELENA directly calculates the current (rather than JETTO), based on the temperature and density profiles provided by JETTO, using the Sauter equation [26,27] for the bootstrap current contribution to the current as this matched the EUROPED methodology in reference [6]. Furthermore, the equilibrium used for these cases was taken from the EUROPED simulations. This ensured the same plasma boundary and poloidal flux mapping between JETTO-MISHKA and EUROPED.
- **S.2** The full model is applied: the temperature, density and current are solved for. $T_{e,sep}$, $T_{i,sep}$ and the poloidally integrated neutral flux ($\Gamma_{sep,neut}$) are taken from EDGE2D-EIRENE simulations [36] (Table 1). The ETB width evolves according to the EPED scaling.
- **S.3** Only the temperature and current profiles are calculated. FRANTIC is operated in feedback mode to produce a user specified $n_{e,ped}$. In this setup, $T_{e,sep} = T_{i,sep} = 100$ eV. The ETB width is either evolved as per the EPED scaling or is fixed by the user.

For each described setup, the coupled codes evolve together over time to convergence, typically about 5-8 s. The transport in the core and the ETB region is given by JETTO (as explained above) with the neutral source provided by FRANTIC and the beam source provided by PENCIL. Periodically (10 times per second), MISHKA calculates the MHD stability of the predicted ETB and the transport in the ETB region is adjusted as described in Section 2.3. We define simulation convergence when $T_{e,ped}$, $T_{i,ped}$ and $n_{e,ped}$ converge to constant values over a time window greater than approximately 1 s. In practise, this means that the final predicted profiles are akin to the experimental pre-ELM profiles; the continuous ELM model has evolved the profiles to the ideal MHD stability boundary.

3. Results

Previous work by reference [6] showed for $n_{e,sep} \leq 1.5\times10^{19}$ m^{-3} that the degradation of $p_{e,ped}$ with $n_{e,sep}$ could be captured using EUROPED. This was achieved with an experimental density profile (fitted using the mtanh method [28]) and rigidly shifting the profile inward and outward with respect to a fixed separatrix position shown in Fig. 1(b) to emulate a change in $n_{e,sep}$. For each density profile, a temperature profile is predicted, and hence a marginally stable pressure pedestal is found from ideal MHD stability analysis. This is the standard workflow of finding a marginally stable pressure pedestal using EPED/EUROPED (i.e. assuming a fixed density profile and predicting the temperature profile). The initial objective of this work was to try to reproduce the degradation of $p_{e,ped}$ throughout the range of $n_{e,sep}$ ($\approx$ 1–4 $\times 10^{19}$ m^{-3}) and not just for $n_{e,sep} \leq 1.5\times10^{19}$ m^{-3}. JINTRAC captures more physics than the standard EPED model (used by reference [6]). In particular it is able to calculate the density profile from first principles. As a result of this, shifts between the positions of the maximum gradients of the temperature and density profile can occur naturally, which have been shown to be important to the pedestal stability [37,38].

Within the JINTRAC model described in Section 2 and the continuous ELM model (Section 2.3), a select few parameters physically dictate the growth of the pedestal: (1) the ratio D/χ, (2) the width of the pedestal (Δ_{ne}), (3) the separatrix values - $T_{e,sep}$, $T_{i,sep}$, $n_{e,sep}$ and (4) neutral influx at separatrix. To investigate the effect of $n_{e,sep}$ on $p_{e,ped}$, and the predicted profiles, all of the above parameters must be set and will therefore impact the trend we are looking for. Thus, in the coming sections, we investigate how each of these parameters both individually and collectively, affect the prediction of $p_{e,ped}$ when $n_{e,sep}$ is varied.

3.1. Comparison between JETTO-MISHKA and EUROPED

As stated previously, reference [6] has shown using EUROPED that degradation of $p_{e,ped}$ is observed only up to $n_{e,sep}$ of $\leq$ 1.5 $\times$ 10^{19} m^{-3}. Here we attempt to replicate these results in JINTRAC using the same methods. JETTO-MISHKA simulations qualitatively show the same trend as the EUROPED results [6], as shown in Fig. 1(c). The degradation of $p_{e,ped}$ is observed up to $n_{e,sep}$ of $\leq$ 1.5 $\times$ 10^{19} m^{-3} in both EUROPED (Fig. 1(c)) and JETTO-MISHKA (Fig. 1(c)). However, above this $n_{e,sep}$ value, neither code shows any further significant degradation of $p_{e,ped}$ compared to the experimental data (small blue circles Fig. 1(c)). The simulation set up of these simulations is described in **S.1**. Note that in order to make a fairer comparison to EUROPED the current profile is calculated in HELENA unlike the rest of the proceeding simulations in which the current is calculated by JETTO. The density profiles in these JETTO simulations were taken directly from the EUROPED runs presented in [6] (Fig. 1(b)) and were kept fixed, only the temperature was evolved (Fig. 1(a)). The pedestal width in these simulations was predicted by the EPED scaling - $\Delta = 0.076\sqrt{(T_{e,ped}\ n_{e,ped}\ /\mu_0\ \bar{B}_p^2)}$ where the Δ is the pedestal width (temperature and density widths are assumed to be the same), μ_0 is the permeability of free space and $\bar{B}_p^2$ is the poloidal field taken at the separatrix. In this simulation set up $T_{e,ped}$ is predicted however, since the density is not being solved for, $n_{e,ped}$ is set to 3.48×10^{19} m^{-3} for all the JETTO-MISHKA simulations (which was also done in EUROPED simulations from reference [6]) shown in Fig. 1(c). In Fig. 1(c) $p_{e,ped}$ of JETTO-MISHKA (circles) and EUROPED runs (linked stars) are shown. The presented $p_{e,ped}$ values in Fig. 1(c) of the EUROPED runs correspond to $p_{e,ped}$ presented in Figure 6b of the Ref. [6]. The legend of Fig. 1(c) lists the most unstable modes for the JETTO-MISHKA runs, which are similar to the EUROPED predictions - $n = 15$ for the lowest $n_{e,sep}$ case and $n = 30$ for the middle and higher $n_{e,sep}$ cases.

The small blue circles featured in the following Figures (including Fig. 1(c)) show fit variables from modified tanh (mtanh) fits [28,29] used to fit the experimental data. Details of the fitting method can be found in Ref. [28]. Importantly, the mtanh fits have been shifted so that the separatrix is assumed to be at 100 eV, which is a standard approximation for JET [36,39]. The experimental data set shown is for JET H-mode low δ plasmas for varying divertor configurations (corner, vertical and horizontal), a range of normalised plasma beta β_n = 1.2–1.9, I_p = 1.9–2.4 MA and B_t = 2.1–2.4 T. Further details of the experimental data can be found in Refs. [6,7].

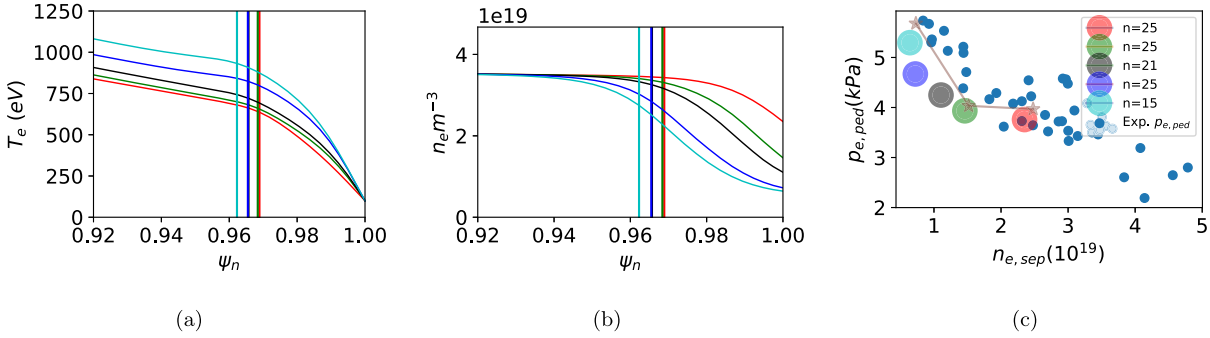

Fig. 1. (a) - JETTO-MISHKA-FRANTIC predictions of the temperature profiles when the density profiles from (b) are input into JETTO and not evolved. The horizontal lines show the predicted width of the ETB (from JETTO) as per the EPED scaling. (c) Qualitative agreement between EUROPED runs (stars) presented in reference [6] and JETTO-MISHKA runs using the density profiles shown in (b). The small blue circles show the experimental data [6].

Table 1
Separatrix values from EDGE2D-EIRENE simulations in reference [36] which are input as boundary conditions into JETTO. Electron separatrix temperatures ($T_{e,sep}$), ion separatrix temperatures ($T_{i,sep}$) and the poloidally integrated atomic neutral flux at the separatrix ($\Gamma_{sep,neut}$), are given as a function of $n_{e,sep}$.

$n_{e,sep}$ (10^{19} m^{-3})	$T_{e,sep}$ (eV)	$T_{i,sep}$ (eV)	$\Gamma_{sep,neut}$ (10^{21} particles s^{-1})
2	113	209	5.03
3	97	170	4.54
4	90	144	5.27
5	85	123	6.44

3.2. Using boundary conditions from EDGE2D-EIRENE in JETTO-MISHKA-FRANTIC

It has been shown that $T_{e,sep}$ and $T_{i,sep}$ vary when a scan in $n_{e,sep}$ is carried out using the scrape off layer transport code, EDGE2D-EIRENE [36] which is to be expected [5]. A scan in $n_{e,sep}$ was performed in EDGE2D-EIRENE where the neutral atomic influx was automatically adjusted to achieve a particular $n_{e,sep}$. EDGE2D-EIRENE simulations were performed for a vertical target JET H-mode plasma and the perpendicular transport was assumed to be constant throughout the $n_{e,sep}$ scan. Table 1 shows the predicted values from EDGE2D-EIRENE of $T_{e,sep}$, $T_{i,sep}$ and the poloidally integrated neutral source at the separatrix ($\Gamma_{sep,neut}$), as a function of $n_{e,sep}$. These predicted values are used as the boundary conditions for a scan in $n_{e,sep}$ from 2–5$\times 10^{19}$ m^{-3} in JETTO-MISHKA-FRANTIC. The ETB width in these simulations was set by the EPED scaling [17]. The simulation set-up used for these cases is described in **S.2**.

When accounting for how $T_{e,sep}$, $T_{i,sep}$ and $\Gamma_{sep,neut}$ varies with $n_{e,sep}$, informed by EDGE2D-EIRENE, the experimental trend of $p_{e,ped}$ degrading with $n_{e,sep}$ is not recovered (stars compared to small blue circles Fig. 2(c)). As $n_{e,sep}$ increases, $n_{e,ped}$ increases almost linearly (Fig. 2(b)), which is not in line with the experimental data. This meant that $p_{e,ped}$ increases at approximately the same rate as $n_{e,ped}$ until it saturates at the highest $n_{e,sep}$, as the change in $T_{e,ped}$ is negligible (Fig. 2(a)), and hence why $p_{e,ped}$ increases with $n_{e,sep}$ (Fig. 2(c)). The change in the width of the ETB (in JETTO) with $n_{e,sep}$ is negligible and underpredicts the mtanh pedestal width (Fig. 2d & e). All these simulations were limited by $n = 25$ ballooning modes.

3.3. Sensitivity of $p_{e,ped}$ to the D/χ ratio

A free parameter within the JETTO-MISHKA-FRANTIC model is the D/χ ratio. For $n_{e,sep} = 2$ & 4×10^{19} m^{-3} JETTO-MISHKA-FRANTIC simulations, using the same simulation set-up as in Section 3.2 (i.e. **S.2**), were run with $D/\chi = 1/20$ and $D/\chi = 1/100$ (Fig. 3). The D/χ ratio is the amount by which transport is modified in the particle channel and heat channels, respectively, by the continuous ELM model. For example, a $D/\chi = 1/20$ which was the ratio used in the previously presented simulations (informed by gyro-kinetic simulations from Ref. [32]), the heat transport χ was increased by a factor 20 more than the transport in the particle channel D, when feeding back on the transport to stay near the ideal PB stability boundary.

In Section 3.2 minimal change in $T_{e,ped}$ is observed over the $n_{e,sep}$ range scanned. Changing D/χ will affect heat transport (χ) and therefore the predicted $T_{e,ped}$. However, a factor 1/5 change in the D/χ ratio had a minimal effect on the predicted $p_{e,ped}$ (Fig. 3(c)) and $T_{e,ped}$ (Fig. 3(a)). It was observed that $p_{e,ped}$ is driven by the same effects as in Section 3.2 i.e. $n_{e,ped}$ increases with $n_{e,sep}$ (Fig. 3(b)) but $T_{e,ped}$ remains approximately constant (Fig. 3(a)). Furthermore, the predicted ETB widths are insensitive the variation in D/χ (Fig. 3(d) & (e)). These simulations were limited by ballooning modes ($n = 25$).

3.4. Using experimental data to further constrain JETTO

Opposite as to what is observed experimentally, in Sections 3.2 and 3.3, as $n_{e,sep}$ is increased, $n_{e,ped}$ is under-predicted and the change in $T_{e,ped}$ is negligible (Fig. 2) leading to $p_{e,ped}$ increasing with $n_{e,sep}$. To more closely follow the experimental data we constrain the following variables in JETTO-MISHKA-FRANTIC to approximately their experimental values: (1) $n_{e,ped}$ as input (rather than using $\Gamma_{sep,neut}$ from EDGE2D-EIRENE), (2) $T_{e,sep} = T_{i,sep} = 100$ eV (rather than from EDGE2D-EIRENE) and (3) the ETB width set fixed at 2.5 cm ($0.041\psi_n$) to closely match the widths of the modified tanh fits (Fig. 2(d) & (e)) rather than using the EPED scaling for the width of the ETB. This is the simulation setup described in **S.3**.

Constraining $n_{e,ped}$ and the ETB width approximately to the experimental values (diamonds Fig. 2(b) & (d) & (e)), the $p_{e,ped}$ degradation with $n_{e,sep}$ is still not observed (Fig. 2(c)). As $n_{e,sep}$ increases, the resulting augmentation in $n_{e,ped}$ coincides with only a slight decrease in $T_{e,ped}$ (Fig. 2a) meaning that $p_{e,ped}$ rises with $n_{e,sep}$, as was observed for the predictive simulations discussed in Section 3.2. These simulations too were also predominately ballooning limited ($n = 21$–25).

3.5. Sensitivity of $p_{e,ped}$ to the ETB width

Varying the pedestal width in JETTO by approximately a factor 3 in real space (approximately a factor 2.5 in ψ_n) showed a reduction in $p_{e,ped}$ of approximately 60% over the $n_{e,sep}$ range 1–3 $\times 10^{19}$ m^{-3}(solid circles Fig. 4(c)) which was a similar change to what was observed experimentally (small blue circles). The ETB width was input into JETTO and varied from 1–3 cm (Fig. 4(d) & (e)) for $n_{e,sep} = 1$–3 $\times$ 10^{19} m^{-3}. Although a similar change in $p_{e,ped}$ was observed between JETTO-MISHKA and the experiment, the ETB widths used in JETTO are far from the experimentally measured (mtanh) pedestal widths (Fig. 4(d) & (e)). The simulation set-up used in these cases is described in **S.3**. Furthermore the low $n_{e,sep}$ case (1×10^{19} m^{-3}) was limited by peeling-ballooning modes ($n = 12$), whereas simulations with higher

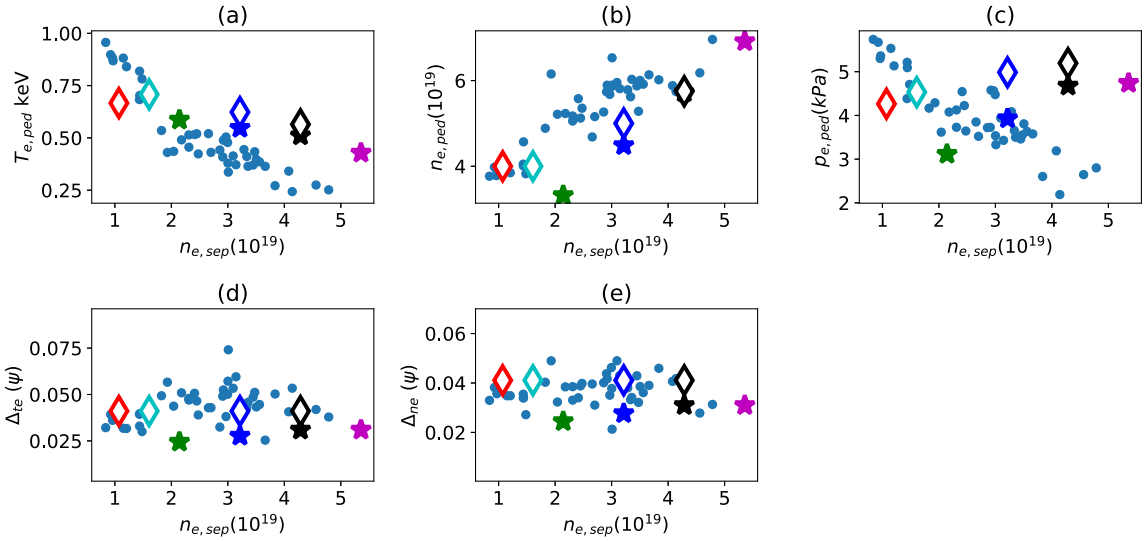

Fig. 2. Variation in pedestal height and width as a function of $n_{e,sep}$ for two sets of JETTO-MISHKA runs. Star markers show JETTO-MISHKA-FRANTIC simulations which use the EDGE2D-EIRENE boundary conditions from Table 1 and the EPED scaling was used for the ETB width. The diamond markers show JETTO-MISHKA-FRANTIC simulations where the ETB width is fixed and $T_{e,sep} = T_{i,sep} = 100$ eV. The small blue circles show the experimental data from the modified tanh fits. (a) height of the electron temperature pedestal ($T_{e,ped}$) as a function of electron separatrix density ($n_{e,sep}$), (b) height of the electron density pedestal ($n_{e,ped}$) as a function of $n_{e,sep}$, (c) height of the electron pressure pedestal ($p_{e,ped}$) as a function of $n_{e,sep}$, (d) width of the electron temperature pedestal (Δ_{te}) in poloidal flux as a function of $n_{e,sep}$ and (e) width of the electron density pedestal Δ_{ne} in poloidal flux as a function of $n_{e,sep}$.

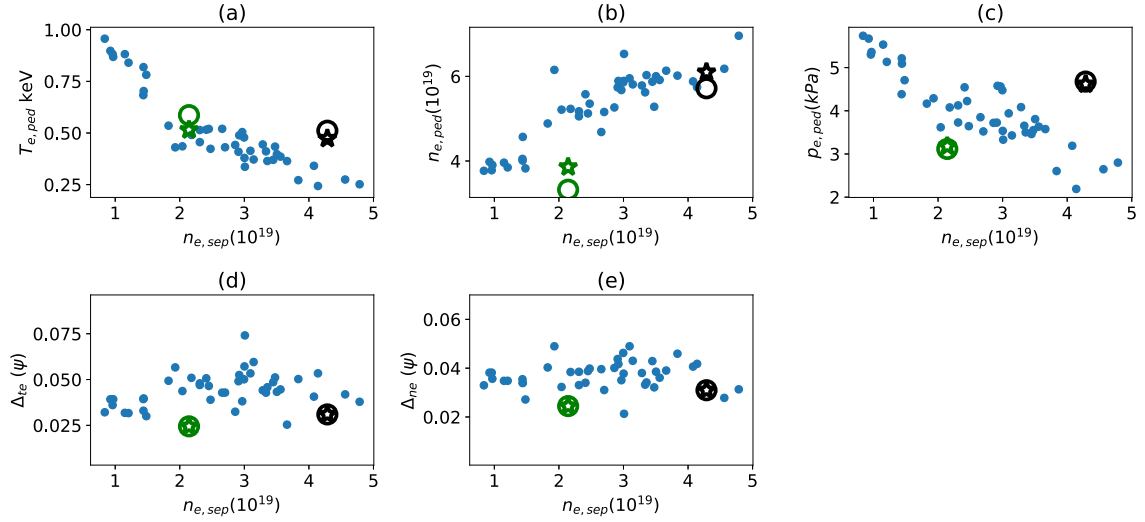

Fig. 3. JETTO-MISHKA-FRANTIC simulations showing the dependence of the pedestal parameters on the chosen D/χ ratio, $D/\chi = 1/100$ (stars) and $D/\chi = 1/20$ (circles), which is the D/χ ratio used in all other plots showing JETTO-MISHKA-FRANTIC simulations. (a) height of the electron temperature pedestal ($T_{e,ped}$) as a function of electron separatrix density ($n_{e,sep}$), (b) height of the electron density pedestal ($n_{e,ped}$) as a function of $n_{e,sep}$, (c) height of the electron pressure pedestal ($p_{e,ped}$) as a function of $n_{e,sep}$, (d) width of the electron temperature pedestal (Δ_{te}) in poloidal flux as a function of $n_{e,sep}$ and (e) width of the electron density pedestal Δ_{ne} in poloidal flux as a function of $n_{e,sep}$.

$n_{e,sep}$ were ballooning limited ($n = 25$). Note that the case at $n_{e,sep} = 4\times10^{19}$ m^{-3} is not shown in Fig. 4 due to computational convergence issues.

4. Discussion and conclusion

The motivation of these simulations was to apply a model to the pedestal that potentially could capture more physics than the typical pedestal stability analysis usually conducted on JET H-mode plasmas, such as the prediction of a self-consistent density pedestal. Qualitative agreement between JETTO-MISHKA and EUROPED (for $n_{e,sep} \leq 1.5\times10^{19}$ m^{-3}) was observed when the density profile was input into JETTO. In these cases, we were only able to observe the degradation for $n_{e,sep} \leq 1.5\times10^{19}$ m^{-3}, in agreement with the results from EUROPED (Fig. 1(c)). This is also consistent with the previously published work presented in Figure 6(b) in Ref. [6] in which the density pedestal was also not predicted. The JETTO-MISHKA-FRANTIC model, which predicts the density pedestal was not able to recover degradation of $p_{e,ped}$ with $n_{e,sep}$ when using separatrix boundary conditions from EDGE2D-EIRENE (Table 1) and using the EPED scaling to predict the ETB width (Fig. 2). Within these simulations, $p_{e,ped}$ increased with $n_{e,sep}$, which was predominately driven by an increase in $n_{e,ped}$ with $n_{e,sep}$ and a negligible change in $T_{e,ped}$, whereas experimentally $T_{e,ped}$ degrades with $n_{e,sep}$. In an attempt to change $T_{e,ped}$, in the simulations, the transport was changed by increasing the D/χ ratio from 1/20 to 1/100. However this had a minimal change on the predicted $T_{e,ped}$ and hence $p_{e,ped}$ (Fig. 3). Furthermore, $n_{e,ped}$ has been under-predicted (Fig. 2(b), star markers) when using $\Gamma_{sep,neut}$. So, $n_{e,ped}$ was set to approximately follow the experimental data, but again no degradation of $p_{e,ped}$ was observed with $n_{e,sep}$ (diamonds Fig. 2). In fact, the only parameter found to cause

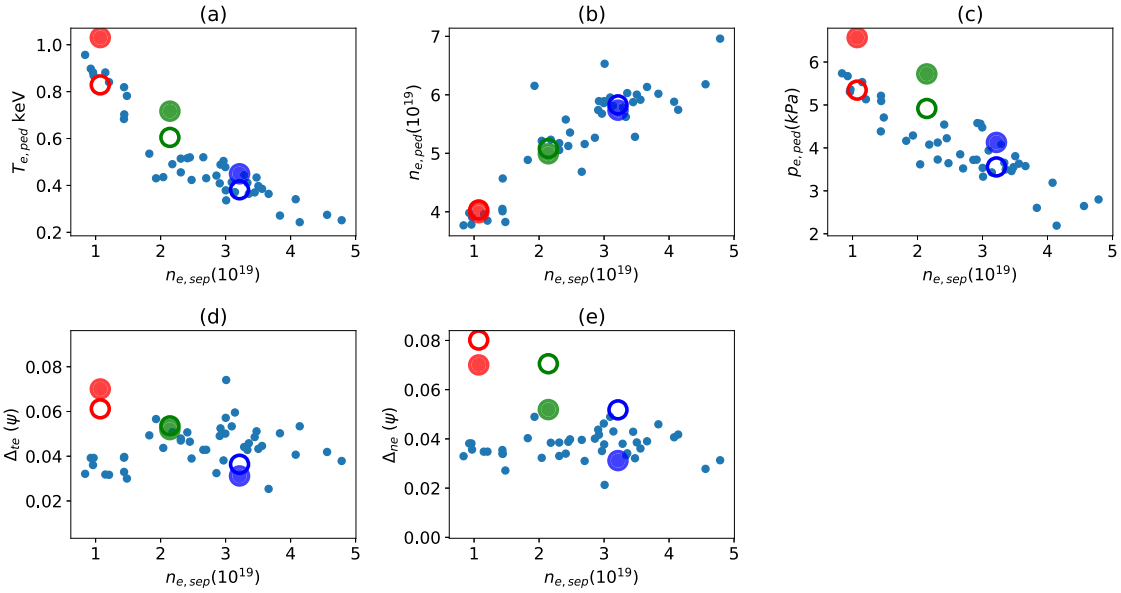

Fig. 4. A scan in the ETB width in JETTO-MISHKA-FRANTIC where the ETB width decreases with $n_{e,sep}$ (panels (d) and (e) - solid circle markers). The JETTO-MISHKA-FRANTIC simulations were configured so that $n_{e,ped}$ is input to closely follow the experimental data, from the modified mtanh fit, (small blue circles) and $T_{e,sep} = T_{i,sep} = 100$ eV (simulation setup S.3). The open circle markers are values of the mtanh fit [28] of the JETTO profiles. (a) height of the electron temperature pedestal ($T_{e,ped}$) as a function of electron separatrix density ($n_{e,sep}$), (b) height of the electron density pedestal ($n_{e,ped}$) as a function of $n_{e,sep}$, (c) height of the electron pressure pedestal ($p_{e,ped}$) as a function of $n_{e,sep}$, (d) width of the electron temperature pedestal (Δ_{te}) in poloidal flux as a function of $n_{e,sep}$ and (e) width of the electron density pedestal Δ_{ne} in poloidal flux as a function of $n_{e,sep}$.

any noticeable $p_{e,ped}$ degradation – approximately 60% – was the ETB width. However, only when varied by a factor of 2.5 (Fig. 4), which is not consistent with the experimentally observed change in the pedestal (mtanh) width (in either the temperature or density). Moreover, the EPED scaling, which has been used to predict the width of the ETB for most of these simulations, routinely underestimates the width of the pedestal compared to the experimental data [7]. This is also evident in the previously presented Figs. 2 & 3 when comparing the predicted ETB width of JETTO-MISHKA-FRANTIC with the experimental data.

Figure 11 in Ref. [6] showed that the ratio of the predicted (from ideal MHD modelling) pedestal pressure gradient (α_{crit}) to the experimentally measured pedestal pressure gradient (α_{exp}) increases from 1 (i.e. ideal MHD model reproduces experimental pressure gradient well) for $n_{e,sep} \leq 1.5 \times 10^{19}$ m^{-3} to approximately 2.5 (i.e. ideal MHD model reproduces experimental pressure gradient poorly) for $n_{e,sep} \approx 4 \times 10^{19}$ m^{-3}. This points to the fact that ideal MHD is not the limiting mechanism of pedestal growth above $n_{e,sep} = 1.5 \times 10^{19}$ m^{-3}. Experimentally it has been observed that the resistivity in the pedestal increases with $n_{e,sep}$ [6]. This means that resistive MHD effects may be important and that the ideal MHD model would not adequately capture the evolution of the pedestal. Modelling by Ref. [40] showed the importance of using resistive MHD stability analysis in order to recover the experimental pressure gradient (α_{exp}). In these aforementioned studies, it is assumed that the shape of the pedestal profile is a modified tanh shape [28,29] and the fit parameters (of the mtanh fit) are used to change height and width of the pedestal profiles. However, in JETTO the shape of the pedestal profile is determined by the choice of D and χ. In the pedestal (or ETB region) this is controlled automatically by the continuous ELM model (described in Section 2.3). The D and χ are set by the continuous model, which varies them based on whether the pedestal is ideal MHD unstable or stable. This different assumption of the shape of the profile can result in different positions of the maximum gradient in JETTO and in other codes, (e.g. EUROPED) which assume a modified tanh (for similar input parameters such as $n_{e,sep}$). This can impact the ideal MHD stability of the pedestal and subsequently the predicted unstable toroidal modes. There has been work using other fitting functions other than the modified tanh to fit the pedestal experimental data, however, these functions were not tested in ideal MHD pedestal stability analysis [41]. To summarise, the assumption of mtanh profiles in [6] means that our use of an ideal MHD model within JINTRAC was still valid for this study, to see if the relaxation of the mtanh assumption could allow us to reproduce the experimental pressure drop for $n_{e,sep} > 1.5 \times 10^{19}$ m^{-3}. The fact that it did not, does lend further support to the use of resistive MHD models in future applications of the JINTRAC code to this problem.

In addition, the current is calculated differently in JETTO compared to HELENA, and hence EUROPED and similar codes. JETTO does not assume the current is fully diffused like HELENA and the bootstrap current in JETTO is calculated by the neoclassical solver (NCLASS), whereas in HELENA it is calculated by the Sauter bootstrap current formula [26,27]. When running JETTO simulations, large edge currents can be driven either by large gradients in the pressure close to the separatrix (which is normally avoided when assuming a mtanh shape) or if the current is not fully diffused in the pedestal region. Although this was not observed in the presented work, it should be considered for future uses of JETTO-MISHKA. Furthermore, it is known that increasing the maximum mode number to $n = 60$ can reduce the predicted $p_{e,ped}$ [3]. Nevertheless, all of these presented simulations have been run to a maximum of $n = 25$, this has been mostly due to restricted computational resources. Predominately, the simulations presented have been unstable to $n = 25$.

In the presented experimental data in Figs. 2, 3 & 4 (small blue circles), the separatrix is assumed to be at the 100 eV point in the electron temperature profile. The fitted mtanh profiles are shifted so that separatrix (i.e. $\psi_n = 1$) is at that point, thus defining the experimental $T_{e,sep}$ and $n_{e,sep}$. This poses two issues when comparing the experimental data to JETTO. Firstly in Sections 3.2 and 3.3 the presented simulations used $T_{e,sep}$ predicted by EDGE2D-EIRENE. These $T_{e,sep}$ values evolved with $n_{e,sep}$ (Table 1) and deviate from 100 eV. Secondly, in all the presented simulations, the definition of the width

of the ETB region in JETTO (where the edge transport is modified to keep the simulation marginally stable) is measured from its innermost edge to the separatrix (i.e. the distance from the top of the pedestal to separatrix). However, this does not necessarily coincide with the mtanh width, in part because some varying fraction of the fitted profile width falls outside of the separatrix (when the profile is shifted). In Fig. 4, the open circle markers show the pedestal heights (Fig. 4(a), (b) & (c)) and widths (Fig. 4(d) & (e)) from the mtanh function [28] when fitted to the predicted electron temperature and density profiles from JETTO (solid circles Fig. 4). It is observed that the mtanh fit predicts different values for $T_{e,ped}$, $n_{e,ped}$, $p_{e,ped}$, Δ_{ne} and Δ_{te} than JETTO, however, the trend with $n_{e,sep}$ in all these variables remains the same between the mtanh fit and JETTO.

In summary, qualitative agreement of the reduction of $p_{e,ped}$ with $n_{e,sep}$ between JETTO-MISHKA and EUROPED has been observed for $n_{e,sep} \leq 1.5 \times 10^{19}$ m^{-3}. Using boundary conditions from EDGE2D-EIRENE simulations, namely $T_{e,sep}$, $T_{i,sep}$, $n_{e,sep}$ and $\Gamma_{sep,neut}$ in JETTO was not able to recover the $p_{e,ped}$ degradation with $n_{e,sep}$ when $n_{e,sep}$ was scanned in JETTO-MISHKA-FRANTIC. Only by changing the pedestal width by a factor 3 in real space was any appreciable drop in $p_{e,ped}$ observed ($\approx 60\%$ compared to the factor two change in the experiment). However, this large change in pedestal width was not supported by the experimental data. Future work should consider (i) the impact of the shape of the profile on the stability, (ii) using different models for the ETB widths in JETTO [7,18] (iii) the use of resistive MHD to limit the pedestal growth rather than ideal MHD [6,40] and, (iv) a benchmark of the current profiles between JETTO and HELENA.

CRediT authorship contribution statement

All simulations were carried out by J. Simpson with the support of their PhD supervisors D. Moulton, C. Giroud and M. Groth. The text was written and proofread by J. Simpson with support from his PhD supervisors. Further advisory support was given by all other co-authors. Furthermore, A. Chankin provided simulations data and L. Frassinetti provided experimental data which was used for comparison to simulation and data for the simulations.

Declaration of competing interest

The authors declare that they have no known competing financial interests or personal relationships that could have appeared to influence the work reported in this paper.

Data availability

Data will be made available on request.

Acknowledgements

This work has been carried out within the framework of the EUROfusion Consortium, funded by the European Union via the Euratom Research and Training Programme (Grant Agreement No 101052200 — EUROfusion). Views and opinions expressed are however those of the author(s) only and do not necessarily reflect those of the European Union or the European Commission. Neither the European Union nor the European Commission can be held responsible for them. (Please mind the addendum 2019–2020)

References

[1] X. Garbet, P. Mantica, F. Ryter, G. Cordey, F. Imbeaux, C. Sozzi, A. Manini, E. Asp, V. Parail, R. Wolf, Profile stiffness and global confinement, Plasma Phys. Control. Fusion (ISSN: 07413335) 46 (9) (2004) 1351–1373, http://dx.doi.org/10.1088/0741-3335/46/9/002, [Online]. Available: https://iopscience.iop.org/article/10.1088/0741-3335/46/9/002https://iopscience.iop.org/article/10.1088/0741-3335/46/9/002/meta.

[2] ITER physics Experts, Chapter 2 : Plasma confinement and transport, vol. 39, no. 12.

[3] C. Maggi, S. Saarelma, F. Casson, C. Challis, E. de la Luna, L. Frassinetti, C. Giroud, E. Joffrin, J. Simpson, M. Beurskens, I. Chapman, J. Hobirk, M. Leyland, P. Lomas, C. Lowry, I. Nunes, F. Rimini, A. Sips, H. Urano, Pedestal confinement and stability in JET-ILW ELMy H-modes, Nucl. Fusion (ISSN: 0029-5515) 55 (11) (2015) 113031, http://dx.doi.org/10.1088/0029-5515/55/11/113031, [Online]. Available:http://iopscience.iop.org/article/10.1088/0029-5515/55/11/113031.

[4] S.I. Krasheninnikov, A.S. Kukushkin, Physics of ultimate detachment of a tokamak divertor plasma, J. Plasma Phys. 83 (5) (2017) 155830501, http://dx.doi.org/10.1017/S0022377817000654.

[5] P.C. Stangeby, The Plasma Boundary of Magnetic Fusion Devices, Institute of Physics, 2000.

[6] L. Frassinetti, C. Perez Von Thun, B. Chapman, A. Fil, J.C. Hillesheim, L. Horvath, G.T. Huijsmans, H. Nyström, V. Parail, S. Saarelma, G. Szepesi, B. Viola, R. Bianchetti Morales, M. Dunne, A.R. Field, J. Flanagan, J.M. Fontdecaba, D. Hatch, B. Lomanowski, C.F. Maggi, S. Menmuir, S. Pamela, C.M. Roach, E. Rachlew, E.R. Solano, Jet Contributors, Role of the separatrix density in the pedestal performance in deuterium low triangularity JET-ILW plasmas and comparison with JET-C, Nucl. Fusion (ISSN: 17414326) 61 (12) (2021) http://dx.doi.org/10.1088/1741-4326/ac3363.

[7] L. Frassinetti, S. Saarelma, G. Verdoolaege, M. Groth, J.C. Hillesheim, P. Bilkova, P. Bohm, M. Dunne, R. Fridström, E. Giovannozzi, F. Imbeaux, B. Labit, E. De La Luna, C. Maggi, M. Owsiak, R. Scannell, Pedestal structure, stability and scalings in JET-ILW: The EUROfusion JET-ILW pedestal database, Nucl. Fusion (ISSN: 17414326) 61 (1) (2021) http://dx.doi.org/10.1088/1741-4326/abb79e.

[8] M.G. Dunne, S. Potzel, F. Reimold, M. Wischmeier, E. Wolfrum, L. Frassinetti, M. Beurskens, P. Bilkova, M. Cavedon, R. Fischer, B. Kurzan, F.M. Laggner, R.M. McDermott, G. Tardini, E. Trier, E. Viezzer, M. Willensdorfer, The role of the density profile in the ASDEX-Upgrade pedestal structure, Plasma Phys. Control. Fusion (ISSN: 13616587) 59 (1) (2017) http://dx.doi.org/10.1088/0741-3335/59/1/014017.

[9] J. Canik, et al., Impact of Closure on the Deeply Detached Divertor in DIII-D, American Physical Society (APS-DPP), 2022.

[10] J.W. Connor, Edge-localized modes - physics and theory, Plasma Phys. Control. Fusion 40 (1997) 531–542.

[11] S. Saarelma, a. Alfier, M.N.a. Beurskens, R. Coelho, H.R. Koslowski, Y. Liang, I. Nunes, MHD stability analysis of small ELM regimes in JET, Plasma Phys. Control. Fusion (ISSN: 0741-3335) 51 (3) (2009) 035001, http://dx.doi.org/10.1088/0741-3335/51/3/035001, [Online]. Available:http://stacks.iop.org/0741-3335/51/i=3/a=035001?key=crossref.cb533bb78aeb89cab2ac59765e0cfb77.

[12] P. Snyder, N. Aiba, M. Beurskens, R. Groebner, L. Horton, a. Hubbard, J. Hughes, G. Huysmans, Y. Kamada, a. Kirk, C. Konz, a. Leonard, J. Lönnroth, C. Maggi, R. Maingi, T. Osborne, N. Oyama, a. Pankin, S. Saarelma, G. Saibene, J. Terry, H. Urano, H. Wilson, Pedestal stability comparison and ITER pedestal prediction, Nucl. Fusion (ISSN: 0029-5515) 49 (2009) 085035, http://dx.doi.org/10.1088/0029-5515/49/8/085035, [Online]. Available:http://stacks.iop.org/0029-5515/49/i=8/a=085035?key=crossref.fb4fb424d51522213b8d424d5b0e4372.

[13] P.B. Snyder, H.R. Wilson, J.R. Ferron, L.L. Lao, a.W. Leonard, T.H. Osborne, a.D. Turnbull, D. Mossessian, M. Murakami, X.Q. Xu, Edge localized modes and the pedestal: A model based on coupled peeling–ballooning modes, Phys. Plasmas (ISSN: 1070664X) 9 (5) (2002) 2037, http://dx.doi.org/10.1063/1.1449463, [Online]. Available:http://scitation.aip.org/content/aip/journal/pop/9/5/10.1063/1.1449463.

[14] H.R. Wilson, P.B. Snyder, G.T.a. Huysmans, R.L. Miller, Numerical studies of edge localized instabilities in tokamaks, Phys. Plasmas (ISSN: 1070664X) 9 (4) (2002) 1277, http://dx.doi.org/10.1063/1.1459058, [Online]. Available:http://scitation.aip.org/content/aip/journal/pop/9/4/10.1063/1.1459058.

[15] A. Mikhailovskii, G. Huysmans, W. Kerner, S. Sharapov, Optimization of computational MHD normal-mode analysis for tokamaks, Plasma Phys. Rep. (ISSN: 1063-780X) 23 (1997) 844–857, http://dx.doi.org/10.1134/1.952514, [Online]. Available:https://inis.iaea.org/search/search.aspx?orig_q=RN:35015207.

[16] S. Saarelma, C.D. Challis, L. Garzotti, L. Frassinetti, C.F. Maggi, M. Romanelli, C. Stokes, Integrated modelling of H-mode pedestal and confinement in JET-ILW, Plasma Phys. Control. Fusion (ISSN: 13616587) 60 (1) (2018) http://dx.doi.org/10.1088/1361-6587/aa8d45.

[17] P.B. Snyder, R.J. Groebner, a.W. Leonard, T.H. Osborne, H.R. Wilson, Development and validation of a predictive model for the pedestal height, Phys. Plasmas (ISSN: 1070664X) 16 (2009) 056118, http://dx.doi.org/10.1063/1.3122146, [Online]. Available:http://scitation.aip.org/content/aip/journal/pop/16/5/10.1063/1.3122146.

[18] T. Luda, C. Angioni, M.G. Dunne, E. Fable, A. Kallenbach, N. Bonanomi, P.A. Schneider, M. Siccinio, G. Tardini, Integrated modeling of ASDEX Upgrade plasmas combining core, pedestal and scrape-off layer physics, Nucl. Fusion (ISSN: 17414326) 60 (3) (2020) 036023, http://dx.doi.org/10.1088/1741-4326/ab6c77, [Online]. Available:.

[19] C. Challis, J. Cordey, H. Hamnén, P. Stubberfield, J. Christiansen, E. Lazzaro, D. Muir, D. Stork, E. Thompson, Non-inductively driven currents in JET, Nucl. Fusion (ISSN: 0029-5515) 29 (4) (1989) 563–570, http://dx.doi.org/10.1088/0029-5515/29/4/002, [Online]. Available:https://iopscience.iop.org/article/10.1088/0029-5515/29/4/002.

[20] S. Tamor, ANTIC: A code for calculation of neutral transport in cylindrical plasmas, J. Comput. Phys. (ISSN: 10902716) 40 (1) (1981) 104–119, http://dx.doi.org/10.1016/0021-9991(81)90202-3.

[21] J. Simpson, D. Moulton, C. Giroud, F. Casson, M. Groth, A. Chankin, L. Horvath, D.S. Gahle, L. Garzotti, G. Corrigan, F. Kochl, An examination of the Neutral Penetration Model $1/n_{e,ped}$ scaling for its validity of spatially varying neutral sources, Nucl. Mater. Energy (ISSN: 2352-1791) 28 (2021) 101037, http://dx.doi.org/10.1016/J.NME.2021.101037.

[22] M. Romanelli, G. Corrigan, V. Parail, S. Wiesen, R. Ambrosino, P. Da Silva Aresta Belo, L. Garzotti, D. Harting, F. Köchl, T. Koskela, L. Lauro-Taroni, C. Marchetto, M. Mattei, E. Militello-Asp, M.F.F. Nave, S. Pamela, A. Salmi, P. Strand, G. Szepesi, JINTRAC: A system of codes for integrated simulation of Tokamak scenarios, Plasma Fusion Res. (ISSN: 18806821) 9 (SPECIALISSUE.2) (2014) http://dx.doi.org/10.1585/pfr.9.3403023.

[23] M. Erba, A. Cherubini, V.V. Parail, E. Springmann, A. Taroni, Development of a non-local model for tokamak heat transport in L-mode, H-mode and transient regimes, Plasma Phys. Control. Fusion (ISSN: 0741-3335) 39 (2) (1997) 261, http://dx.doi.org/10.1088/0741-3335/39/2/004, [Online]. Available: https://iopscience.iop.org/article/10.1088/0741-3335/39/2/004https://iopscience.iop.org/article/10.1088/0741-3335/39/2/004/meta.

[24] W.A. Houlberg, K.C. Shaing, S.P. Hirshman, M.C. Zarnstorff, Bootstrap current and neoclassical transport in tokamaks of arbitrary collisionality and aspect ratio, Phys. Plasmas (ISSN: 1070-664X) 4 (9) (1998) 3230, http://dx.doi.org/10.1063/1.872465, [Online]. Available:https://aip.scitation.org/doi/abs/10.1063/1.872465.

[25] G.T.A. Huysmans, J.P. Goedbloed, K. W., HELENA, in: Proceedings CP90 Conference on Computational Physics Proceedings, 1991, p. 371.

[26] O. Sauter, C. Angioni, Y.R. Lin-Liu, Neoclassical conductivity and bootstrap current formulas for general axisymmetric equilibria and arbitrary collisionality regime, Phys. Plasmas 6 (1999) 2834, http://dx.doi.org/10.1063/1.873240, [Online]. Available:.

[27] O. Sauter, C. Angioni, Y.R. Lin-Liu, Erratum: "Neoclassical conductivity and bootstrap current formulas for general axisymmetric equilibria and arbitrary collisionality regime", Phys. Plasmas 9 (2002) 5140, http://dx.doi.org/10.1063/1.1517052, [Online]. Available:.

[28] L. Frassinetti, M.N.a. Beurskens, R. Scannell, T.H. Osborne, J. Flanagan, M. Kempenaars, M. Maslov, R. Pasqualotto, M. Walsh, Spatial resolution of the JET Thomson scattering system, Rev. Sci. Instrum. (ISSN: 1089-7623) 83 (1) (2012) 013506, http://dx.doi.org/10.1063/1.3673467, [Online]. Available:http://www.ncbi.nlm.nih.gov/pubmed/22299950.

[29] R. Scannell, M. Beurskens, P.G. Carolan, A. Kirk, M. Walsh, T. O'Gorman, T.H. Osborne, Deconvolution of Thomson scattering temperature profiles, Rev. Sci. Instrum. (ISSN: 00346748) 82 (5) (2011) http://dx.doi.org/10.1063/1.3581230.

[30] L.L. Lao, H.S. John, R.D. Stambaugh, A.G. Kellman, W. Pfeiffer, Reconstruction of current profile parameters and plasma shapes in tokamaks, Nucl. Fusion 25 (11) (1985) 1611–1622, http://dx.doi.org/10.1088/0029-5515/25/11/007.

[31] C. Angioni, H. Weisen, O.J. Kardaun, M. Maslov, A. Zabolotsky, C. Fuchs, L. Garzotti, C. Giroud, B. Kurzan, P. Mantica, A.G. Peeters, J. Stober, Scaling of density peaking in H-mode plasmas based on a combined database of AUG and JET observations, Nucl. Fusion (ISSN: 0029-5515) 47 (9) (2007) 1326, http://dx.doi.org/10.1088/0029-5515/47/9/033, [Online]. Available: https://iopscience.iop.org/article/10.1088/0029-5515/47/9/033https://iopscience.iop.org/article/10.1088/0029-5515/47/9/033/meta.

[32] M. Kotschenreuther, X. Liu, D.R. Hatch, S. Mahajan, L. Zheng, A. Diallo, R. Groebner, J.C. Hillesheim, C.F. Maggi, C. Giroud, F. Koechl, V. Parail, S. Saarelma, E. Solano, A. Chankin, Gyrokinetic analysis and simulation of pedestals to identify the culprits for energy losses using 'fingerprints', Nucl. Fusion (ISSN: 17414326) 59 (9) (2019) 096001, http://dx.doi.org/10.1088/1741-4326/ab1fa2, [Online]. Available: https://iopscience.iop.org/article/10.1088/1741-4326/ab1fa2https://iopscience.iop.org/article/10.1088/1741-4326/ab1fa2/meta.

[33] V. Parail, P. Belo, P. Boerner, X. Bonnin, G. Corrigan, D. Coster, J. Ferreira, A. Foster, L. Garzotti, G.M. Hogeweij, W. Houlberg, F. Imbeaux, J. Johner, F. Kochl, V. Kotov, L. Lauro-Taroni, X. Litaudon, J. Lonnroth, G. Pereverzev, Y. Peysson, G. Saibene, R. Sartori, M. Schneider, G. Sips, P. Strand, G. Tardini, M. Valovic, S. Wiesen, M. Wischmeier, R. Zagorski, Integrated modelling of ITER reference scenarios, Nucl. Fusion (ISSN: 00295515) 49 (7) (2009) 075030, http://dx.doi.org/10.1088/0029-5515/49/7/075030, Online]. Available: https://iopscience.iop.org/article/10.1088/0029-5515/49/7/075030https://iopscience.iop.org/article/10.1088/0029-5515/49/7/075030/meta.

[34] V. Parail, R. Albanese, R. Ambrosino, J.F. Artaud, K. Besseghir, M. Cavinato, G. Corrigan, J. Garcia, L. Garzotti, Y. Gribov, F. Imbeaux, F. Koechl, C.V. Labate, J. Lister, X. Litaudon, A. Loarte, P. Maget, M. Mattei, D. McDonald, E. Nardon, G. Saibene, R. Sartori, J. Urban, Self-consistent simulation of plasma scenarios for ITER using a combination of 1.5D transport codes and free-boundary equilibrium codes, Nucl. Fusion (ISSN: 0029-5515) 53 (11) (2013) 113002, http://dx.doi.org/10.1088/0029-5515/53/11/113002, [Online]. Available: https://iopscience.iop.org/article/10.1088/0029-5515/53/11/113002https://iopscience.iop.org/article/10.1088/0029-5515/53/11/113002/meta.

[35] J.-S. Lönnroth, V.V. Parail, G. Corrigan, D. Heading, G. Huysmans, A. Loarte, S. Saarelma, G. Saibene, S. Sharapov, J. Spence, Integrated Predictive Modelling of the Effect of Neutral Gas Puffing in ELMy H-Mode Plasmas, Tech. Rep., 2003, pp. 1689–1711.

[36] J. Simpson, D. Moulton, C. Giroud, M. Groth, G. Corrigan, Using EDGE2D-EIRENE to simulate the effect of impurity seeding and fueling on the upstream electron separatrix temperature, Nucl. Mater. Energy (ISSN: 23521791) 20 (June) (2019) 100599, http://dx.doi.org/10.1016/j.nme.2019.02.002, [Online]. Available:.

[37] E. Stefanikova, L. Frassinetti, S. Saarelma, A. Loarte, I. Nunes, L. Garzotti, P. Lomas, F. Rimini, P. Drewelow, U. Kruezi, et al., Effect of the relative shift between the electron density and temperature pedestal position on the pedestal stability in JET-ILW and comparison with JET-C, Nucl. Fusion 58 (5) (2018) 056010.

[38] E. Stefanikova, L. Frassinetti, S. Saarelma, C.P. von Thun, J. Hillesheim, et al., Change in the pedestal stability between JET-C and JET-ILW low triangularity peeling-ballooning limited plasmas, Nucl. Fusion 61 (2) (2020) 026008.

[39] S. Saarelma, A. Järvinen, M. Beurskens, C. Challis, L. Frassinetti, C. Giroud, M. Groth, M. Leyland, C. Maggi, J. Simpson, The effects of impurities and core pressure on pedestal stability in Joint European Torus (JET), Phys. Plasmas (ISSN: 10897674) 22 (5) (2015) http://dx.doi.org/10.1063/1.4921413.

[40] H. Nyström, L. Frassinetti, S. Saarelma, G. Huijsmans, C.P. von Thun, C. Maggi, J. Hillesheim, et al., Effect of resistivity on the pedestal MHD stability in JET, Nucl. Fusion 62 (12) (2022) 126045.

[41] P.A. Schneider, E. Wolfrum, R.J. Groebner, T.H. Osborne, M.N. Beurskens, M.G. Dunne, J.R. Ferron, S. Günter, B. Kurzan, K. Lackner, P.B. Snyder, H. Zohm, Differences in the H-mode pedestal width of temperature and density, Plasma Phys. Control. Fusion (ISSN: 07413335) 54 (10) (2012) http://dx.doi.org/10.1088/0741-3335/54/10/105009.